Supplemental Information

The CUE Domain of Cue1 Aligns

Growing Ubiquitin Chains

with Ubc7 for Rapid Elongation

Maximilian von Delbrück, Andreas Kniss, Vladimir V. Rogov, Lukas Pluska, Katrin Bagola, Frank Löhr, Peter Güntert, Thomas Sommer, and Volker Dötsch
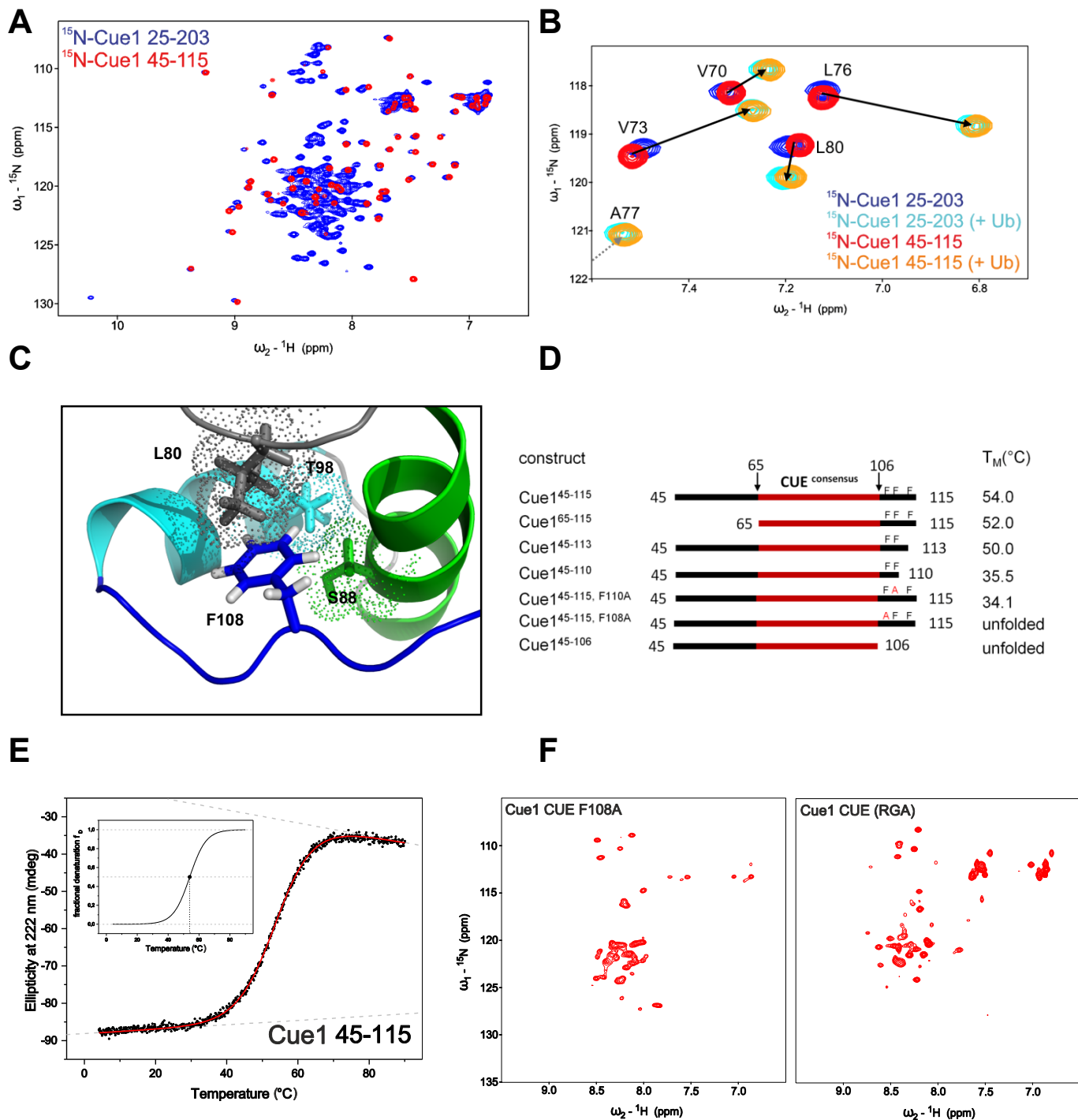
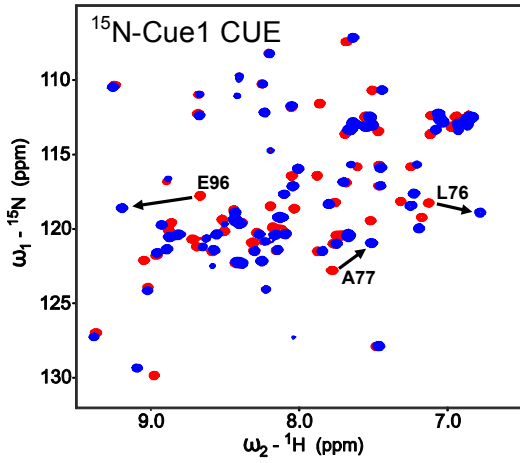# SUPPLEMENTAL FIGURES

Figure S1, related to Figure 1

Figure S2, related to Figure 1
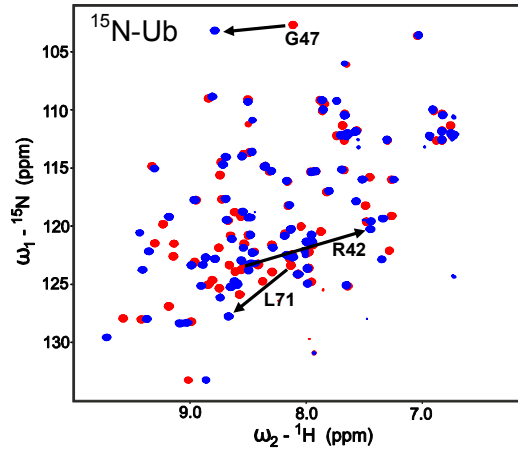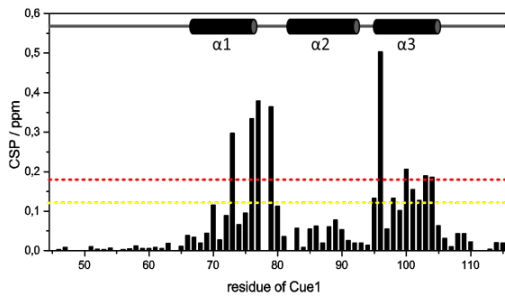
A

B
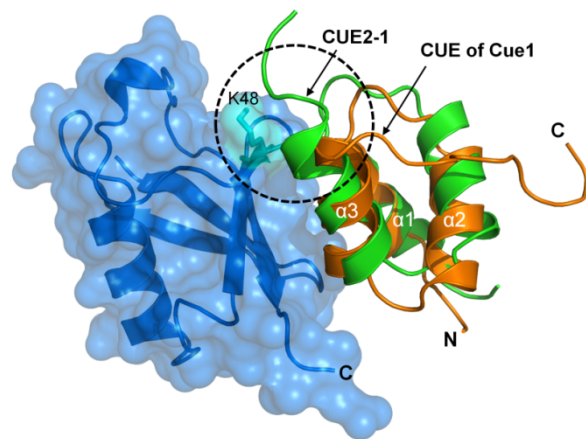
C

D
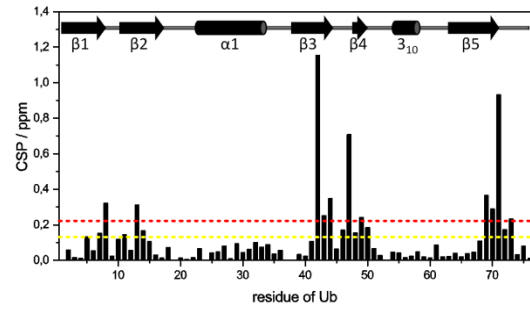
E
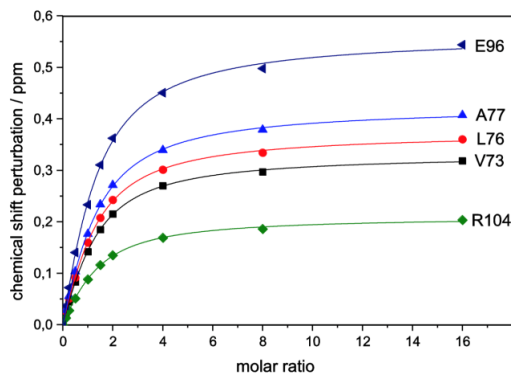
F

Figure S3, related to Figure 1

A

B

time course
K48-Ub$_4$ elongation

time (min): 2   4   7   10   20   40   60

Ub$_5$

Ub

fluorescence scanning

Ub$_4$

coomassie staining

Figure S4, related to Figure 2

A
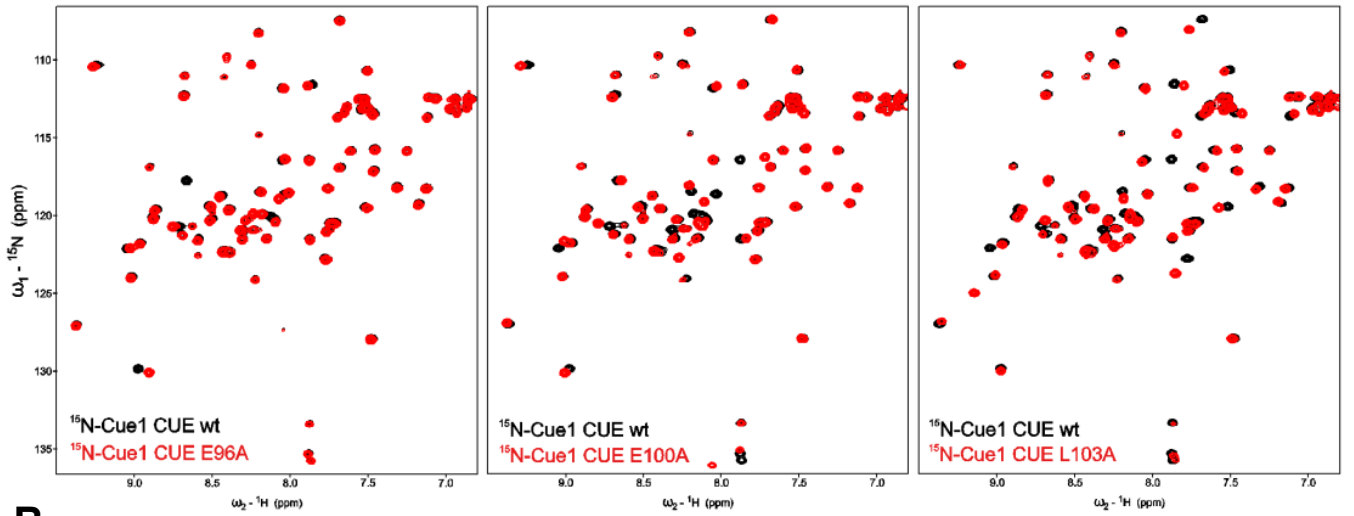
B
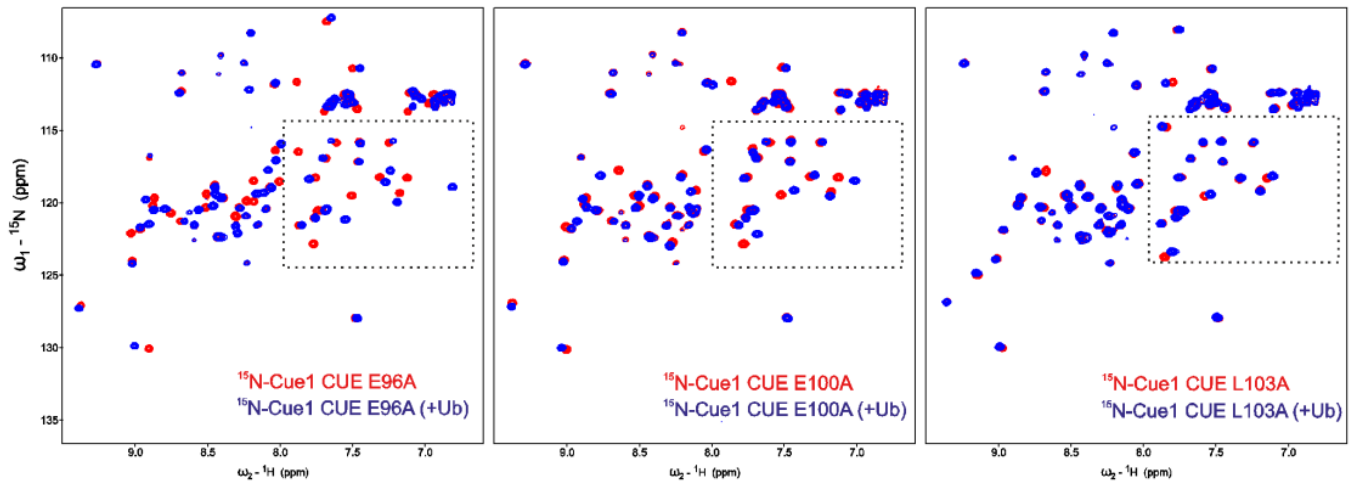
C

Figure S5, related to Figure 3

A

molar ratio Ub:^{15}N-CUE

8 4 2 3/2 1 1/2 1/4 1/8 0

monoUb

118

9.2 9.0 8.8 8.6

E96

K48-Ub$_2$

K48-Ub$_4$

K63-Ub$_2$

K63-Ub$_4$

lin-Ub$_4$

B

RU

140
120
100
80
60
40
20
0
-20

K48-Ub$_4$ (25 µM)
K63-Ub$_4$ (25 µM)
lin-Ub$_4$ (25 µM)
K48-Ub$_2$ (50 µM)
K63-Ub$_2$ (50 µM)

0 50 100 150

time / s

C

steady state RU

100
80
60
40
20
0

Monoubiquitin

Monoubiquitin

0,0 2,0x10^{-4} 4,0x10^{-4} 6,0x10^{-4} 8,0x10^{-4}

ubiquitin concentration / M

D

steady state RU

250
200
150
100
50
0

K48-Ub$_4$

K48-Ub$_4$

0,0 2,0x10^{-4} 4,0x10^{-4} 6,0x10^{-4} 8,0x10^{-4}

ubiquitin concentration / M

E

fluorescence anisotropy

0.17
0.16
0.15
0.14
0.13

K48-Ub$_4$
K48-Ub$_2$

10 20 30 40

time (min)

F

fluorescence anisotropy

0.16
0.15
0.14
0.13
0.12

K63-Ub$_4$
K63-Ub$_2$

10 20 30 40 50 60

time (min)

G

fluorescence intensity band (%)

80
60
40
20
0

K48-linked K63-linked

H

fluorescence anisotropy

0.17
0.16
0.15
0.14
0.13
0.12

K48-Ub$_4$, cCue1
K48-Ub$_2$, cCue1
K48-Ub$_4$, cCue1 RGA
K48-Ub$_2$, cCue1 RGA

10 20 30 40 50 60 70 80

time (min)

I

fluorescence anisotropy

0.16
0.15
0.14
0.13
0.12

K63-Ub$_4$, cCue1 wt
K63-Ub$_2$, cCue1 wt
K63-Ub$_4$, cCue1 RGA
K63-Ub$_2$, cCue1 RGA

10 20 30 40 50 60 70 80

time (min)

J

fluorescence intensity band (%)

80
60
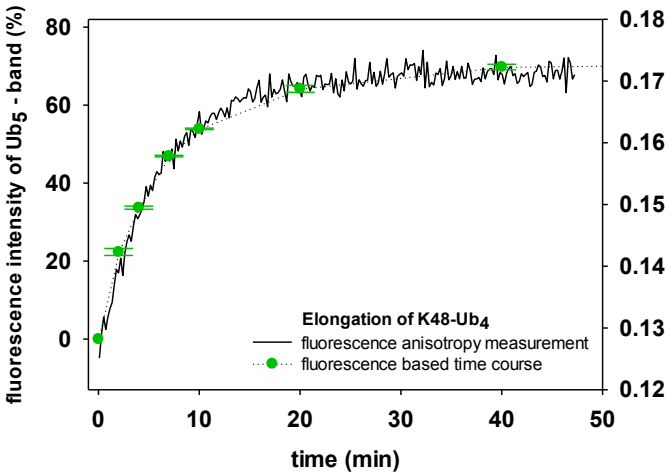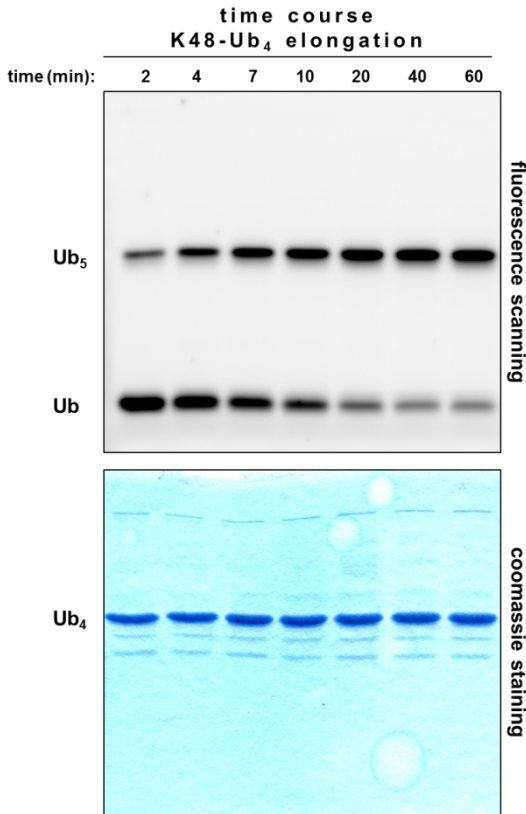40
20
0

cCue1
cCue1 RGA

K48-linked K63-linked

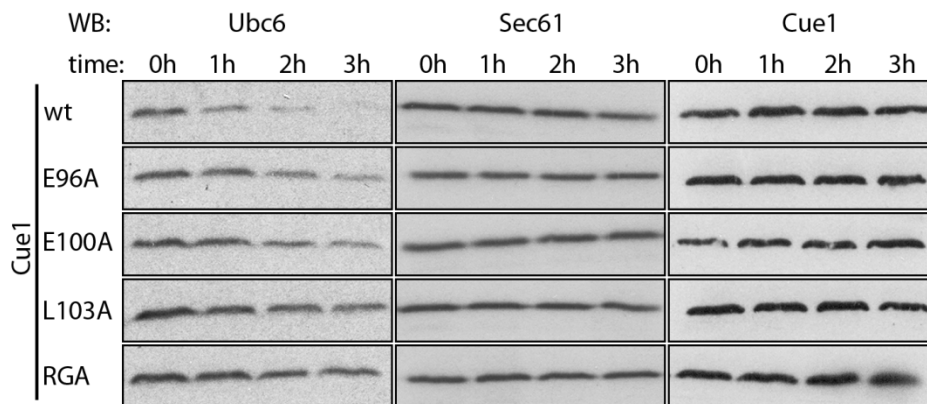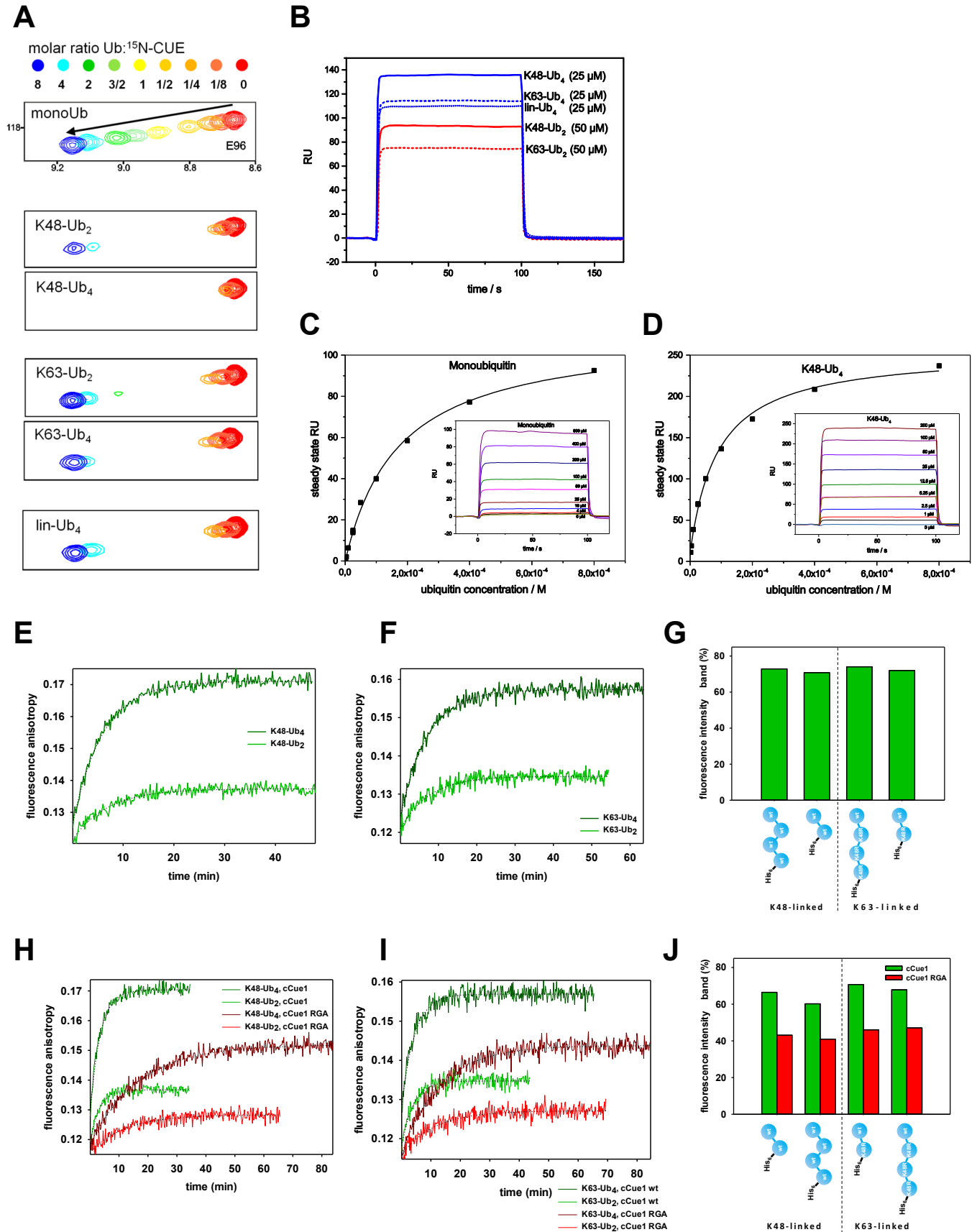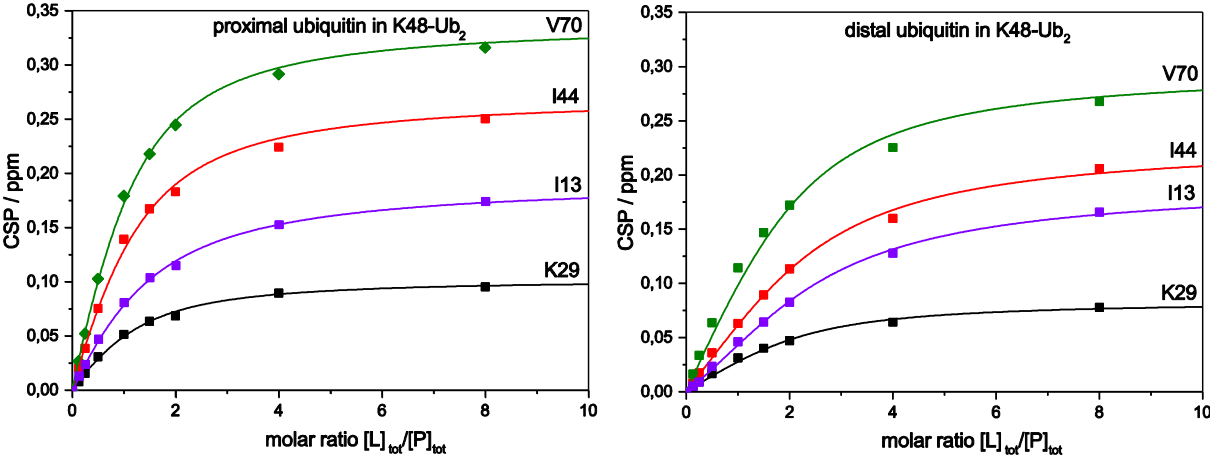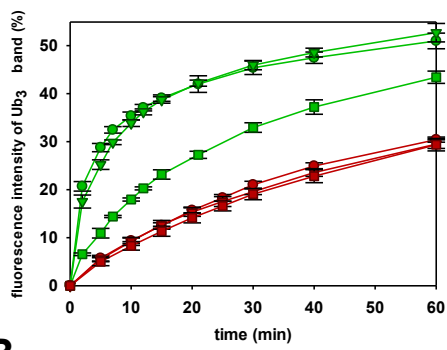**Figure S6, related to Figure 4**

Figure S7, related to Figure 5
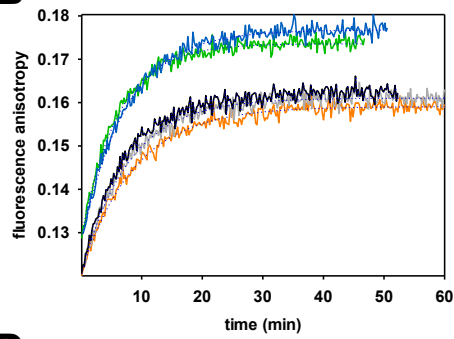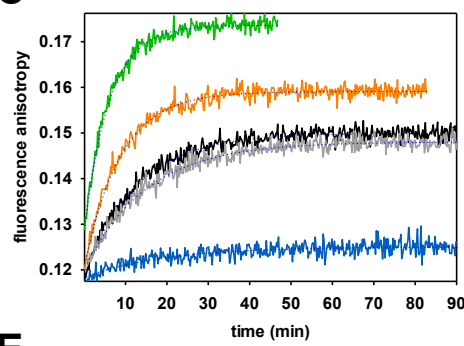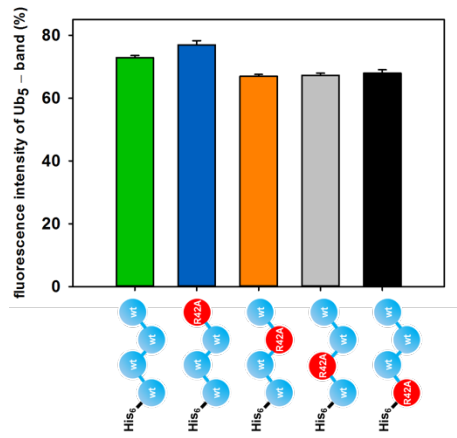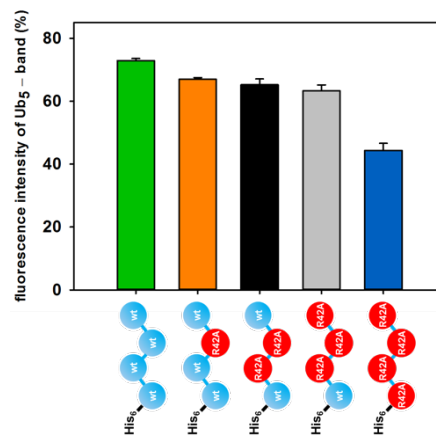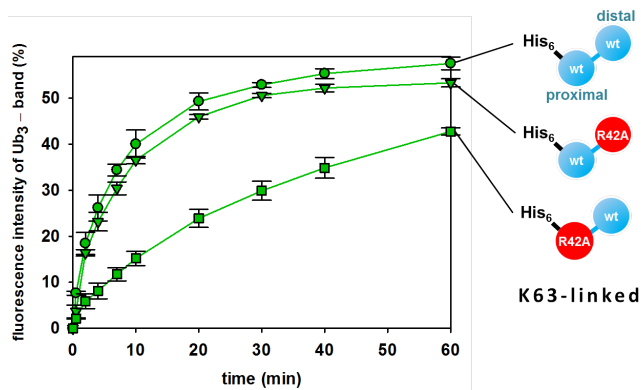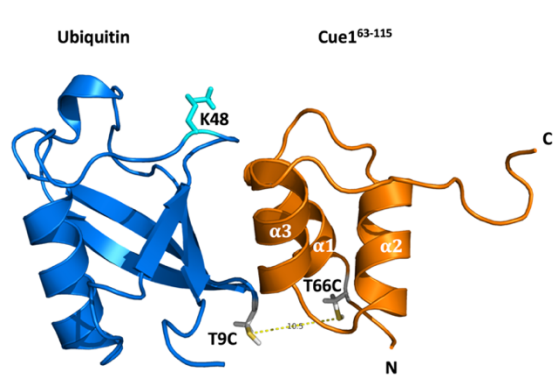
SUPPLEMENTAL FIGURE LEGENDS

Figure S1: Structure and stability of the CUE domain, related to Figure 1

(A) Overlay of [^{15}N,^{1}H]-HSQC spectra of the entire cytosolic Cue1 part (cCue1, 25-203) (blue) and the extended CUE domain (45-115) (red) showing that the well dispersed signals exclusively arise from the CUE domain.

(B) Representative region of HSQC spectra of ^{15}N –labeled Cue1$^{45-115}$ and Cue1$^{25-203}$ (red and blue) as well as spectra of the ubiquitin-bound forms (8-fold molar excess of Ub). Ubiquitin binding activity and CUE domain fold are retained for Cue1$^{45-115}$ as compared to the full length protein.

(C) The F108A side chain is deeply inserted into the hydrophobic core of CUE and interacts with residues from the α1α2 loop (L80), helix α2 (S88) and helix α3 (T98) in order to stabilize the CUE domain.

(D) Overview of all CUE domain constructs used for melting curve analysis by CD spectroscopy. Cue1 features three phenylalanines (F108, F110, F114) beyond the CUE consensus sequence (65-106, shown in red) that significantly contribute to CUE domain stability. By contrast, residues preceding the minimal consensus CUE domain are less important for stabilizing the fold. Melting temperatures obtained by CD analysis are indicated for all CUE constructs except for Cue1$^{45-115,}$ ^{F108A} and Cue1$^{45-106}$ where no comparable transition in the measured ellipticity at 222 nm was detected. These constructs are unfolded under all conditions.

(E) Circular dichroism measured at 222 nm for Cue1$^{45-115}$ as a function of temperature to determine the melting temperature of the CUE domain. The measurements were carried out using a temperature protocol from 4 °C to 90 °C. The raw data (black dots) were fitted assuming a two-state model. Regions preceding and following the unfolding transition were fitted using linear regressions (grey dashed lines). The baseline corrected data showing the exact transition midpoint

is indicated as a small inset. Similar melting curves were measured for all constructs indicated in (D).

(F) HSQC spectra of the F108A and the LAP$^{76-78}$ to RGA$^{76-78}$ variants of the CUE domain showing that both constructs are unfolded.

Figure S2: Interaction between the CUE domain and ubiquitin, related to Figure 1

(A and B) Overlay of ^{15}N-^{1}H HSQC spectra of free (red) and bound forms (blue) of extended CUE domain (A) and ubiquitin (B), respectively. Binding was saturated using a 16-fold molar excess of the unlabeled binding partner.

(C and D) Backbone amide CSP plots of extended CUE domain (C) and ubiquitin (D). The secondary structure elements are shown in both plots revealing the importance of helix α1, the adjacent α1 α2 loop and helix α3 in CUE; and residues within β-strands β3, β4 and β5 in ubiquitin.

(E) CSPs of several residues were analyzed for the Cue1 interaction with monoubiquitin and fitted assuming a 1:1 interaction model. The averaged K_D over all analyzed residues was 152 ± 5 μM.

(F) Comparison of the Cue2/ubiquitin and the Cue1/ubiquitin complexes. Ubiquitin structures of both complexes were superimposed (only one ubiquitin is shown) revealing different orientations of both CUE domains in the complex. The accessibility of ubiquitin residue K48 is differing between both complexes and marked. The C-terminal tip of helix α3 of the CUE2-1 domain of yeast Cue2 (green; PDB: 1OTR) interacts with aliphatic segments of the K48 residue. In contrast, the CUE domain of Cue1 (orange) features a different orientation of its helix α3 followed by its unique C-terminal extension lying on helices α3 and α2.

Figure S3: Fluorescence anisotropy measurements precisely follow ubiquitin chain elongation reactions, related to Figure 1

(A) Correlation of fluorescence anisotropy measurements and fluorescence based time course of elongation of K48-linked tetraubiquitin by cCue1 and Ubc7.

(B) Samples of time course in A were taken at indicated time points and analyzed by SDS-PAGE, fluorescence scanning and Coomassie staining.

Figure S4: The CUE domain variants E96A, E100A and L103A have distinct ubiquitin binding properties and ubiquitin binding activity correlates with ubiquitin chain elongation kinetics and turnover of ERAD substrate Ubc6, related to Figure 2

(A) Overlay of $[^{15}N, {}^{1}H]$-HSQC spectra of Cue1$^{45\text{-}115}$ E96A, E100A and L103A variants (red) and Cue1$^{45\text{-}115}$ wild type (black). Only the mutated and neighboring residues are shifted indicating no structural changes compared to the wild type protein.

(B) Overlay of $[^{15}N, {}^{1}H]$-HSQC spectra of Cue1$^{45\text{-}115}$ E96A, E100A and L103A variants (0.2 mM) in absence (red) and presence (1.6 mM) of ubiquitin (blue). While ubiquitin binding induced significant shifts in the E96A variant, the observed shifts for the E100A and L103A variants were significantly reduced. The framed region is shown in more detail in Figure 2A.

(C) Degradation of Ubc6 was followed after addition of cycloheximide to yeast cells. The amounts of Cue1 variants remained unchanged during the experiments. Sec61 served as loading control. Samples were taken at indicated time points and analyzed by SDS-PAGE and immunoblotting with antibodies against Ubc6, Sec61 and Cue1.

Figure S5: The CUE domain of Cue1 preferentially binds and elongates K48-linked ubiquitin chains, related to Figure 3

(A) NMR titration data showing an overlay of sections representing the backbone amide shift of E96. Spectra were recorded at 9 different Ub:^{15}N-Cue1$^{45\text{-}115}$ molar ratios for different chain types and for monoubiquitin. The Ub:Cue1 molar ratios are indicated as a color code. The titrations show that for shorter chains the interaction is in the intermediate to fast exchange regime while for K48 linked Ub$_4$ chains it is in the intermediate exchange regime, indicating the higher degree of avidity of longer chains.

(B) Surface plasmon resonance (SPR) analysis of the binding of different ubiquitin chains to the CUE domain immobilized on a Biacore SA chip. Since the molecular weight is not dependent on linkage type, differences in steady state response units at the same ubiquitin concentration reflect binding strength. Among measurements of differently linked Ub$_2$ (shown in red) and Ub$_4$ (shown in blue) K48-linked chains consistently yield higher binding levels.

(C) SPR binding experiments of immobilized CUE domain with monoubiquitin. For each experimental series the individual measurements at different ubiquitin concentrations are shown in the insets. The obtained steady state response units were fitted against the apparent concentration of ubiquitin monomer units to obtain the binding constant.

(D) SPR binding experiments of immobilized CUE domain with K48-Ub$_4$.

Elongation kinetics of K48-Ub$_2$ and K48-Ub$_4$ (E, H) and of K63-Ub$_2$ and K63-Ub$_4$ (F, I) restricted for distal elongation (chains with K48R substitutions except for the distal moiety). *In vitro* reactions included E1, Ubc7 and cCue1 (green in E, F, H, I) or cCue1 RGA (red in H, I) and additional cHrd1 (H, I). Samples were taken at the end of elongation reactions and analyzed by SDS-PAGE, fluorescence scanning and Coomassie staining. The quantification of elongation products of reactions in E, F or H, I are summarized in (G) respectively (J).

Figure S6: Comparative analysis of CSPs in proximal and distal moieties of K48-Ub$_2$, related to Figure 4

Titration curves of several representative residues were analyzed for the K48-Ub$_2$ – Cue1 interaction and fitted assuming a binding model with two independent binding sites with different, but invariant affinities (see material and methods).

Figure S7: The binding of the CUE domain adjacent to the acceptor ubiquitin promotes ubiquitin chain elongation, related to Figure 5

(A) Kinetics of diubiquitin elongation by cCue1 (green lines) and cCue1 RGA (red lines) at 10 °C in presence of cHrd1 monitored by time course experiments. Corresponding to reactions without cHrd1 (Figure 5A) cCue1 shows similar kinetics for elongation of wild type diubiquitin (circles) and a variant with distal ubiquitin R42A (inverted triangles). Again, elongation of diubiquitin bearing a proximal ubiquitin R42A variant is significantly slower (squares). In the absence of a functional CUE domain elongation kinetics are independent of the amino acid exchange R42A.

Kinetics of elongation (B, C) and quantification of product pentaubiquitin (D, E) are summarized with same color coding for reactions with K48-Ub$_4$ variants, Ubc7 and cCue1. In (B, D) single R42A amino acid exchanges are introduced in different ubiquitin molecules of tetraubiquitin, whereas (C, E) shows experiments with multiple substitutions in ubiquitin chains.

(F) Ubiquitin chain elongation reactions of K63-linked diubquitin containing R42A. Elongation reactions of K63-linked diubiquitin R42A variants in presence of Ubc7 and cCue1 are followed by time course experiments. Reactions with diubiquitin (circles) and its variant which bears R42A ubiquitin at the distal position (inverted triangles) show similar kinetics. In contrast

elongation is strongly decelerated for R42A placed in the proximal moiety of diubiquitin (squares).

(G) Cartoon representation of the Ub (T9C) – CUE (T66C) complex. Sites for chemical crosslinking using a homobifunctional maleimide containing crosslinker were selected based on the HADDOCK model shown in Figure 1C.

SUPPLEMENTAL TABLES

Table S1: Plasmids used in this study, related to Figure 1-5

Plasmid	Description	Vector	Reference
pMD10	hUb	pETM60	(Rogov et al., 2012)
pMD11	hUb with C-terminal His$_6$-tag (Ub^{6His})	pETM60	this study
pMD12	hUb S20C	pETM60	this study
pMD14	hUb R42A	pETM60	this study
pMD15	hUb R42A with C-terminal His$_6$-tag	pETM60	this study
pMD16	hUb K48R	pETM60	this study
pMD17	hUb K48R with C-terminal His$_6$-tag	pETM60	this study
pMD18	hUb K63R	pETM60	this study
pMD20	linear Ub$_4$	pET39b(+)	(Rogov et al., 2012)
pMD35	hUb T9C	pETM60	this study
pMD36	hUb T9C with C-terminal His$_6$-tag	pETM60	this study
pTX410	Cue1ΔTM (residues 24-203) with C-terminal His$_6$-tag; alias cCue1	pGEX6P1	(Bagola et al., 2013)
pMD23	cCue1 E96A; derived from pTX410	pGEX6P1	this study
pMD24	cCue1 E100A; derived from pTX410	pGEX6P1	this study
pMD25	cCue1 L103A; derived from pTX410	pGEX6P1	this study
pTX411	cCue1 L,A,P76,77,78R,G,A; derived from pTX410	pGEX6P1	(Bagola et al., 2013)
pMD37	cCue1 T66C C147S	pGEX6P1	this study
pTX397	Cue1; bp -450 bis +609	pRS415	(Bagola et al., 2013)
pLP22	Cue1 E96A, derived from pTX397	pRS415	this study
pLP23	Cue1 E100A, derived from pTX397	pRS415	this study
pLP24	Cue1 L103A, derived from pTX397	pRS415	this study
pTX386	Cue1 L,A,P76,77,78R,G,A, derived from pTX397	pRS415	(Bagola et al., 2013)
pAK1	Cue1 (residues 45-115) with N-terminal TEV cleavable modified Ubiquitin (Ub19 tag, (Rogov et al., 2012)	pET39b(+)	this study
pAK2	Cue1 (residues 25-203, C147S) with C-terminal His$_6$-tag	pET39b(+)	this study
pAK3	Cue1 (residues 59-115) with Ub19 tag	pET39b(+)	this study
pAK4	Cue1 (residues 59-115) with Ub19 tag	pET39b(+)	this study
pAK5	Cue1 (residues 62-115) with Ub19 tag	pET39b(+)	this study
pAK6	Cue1 (residues 65-115) with Ub19 tag	pET39b(+)	this study
pAK7	Cue1 (residues 45-113) with Ub19 tag	pET39b(+)	this study
pAK8	Cue1 (residues 45-110) with Ub19 tag	pET39b(+)	this study
pAK9	Cue1 (residues 45-106) with Ub19 tag	pET39b(+)	this study
pAK10	Cue1 E96A (residues 45-115)	pET39b(+)	this study
pAK11	Cue1 E100A (residues 45-115)	pET39b(+)	this study
pAK12	Cue1 L103A (residues 45-115)	pET39b(+)	this study
pAK13	Cue1 F110A (residues 45-115)	pET39b(+)	this study
pAK14	Cue1 (residues 59-115) with N-terminal biotinylation site	pET39b(+)	this study
pTX481	Ube1 (hE1)	pET21d	(Berndsen & Wolberger, 2011)
pTX249	Ubc7 (residues 2-165)	pGEX6P1	(Bagola et al., 2013)
pTX315	Hrd1 (residues 325-550)	pGEX6P1	(Bagola et al., 2013)
pMD26	Cdc34	pGEX6p1	
pMD28	Ubc13	pGEX6p1	(Mansour et al., 2014)
pMD29	Uev1a	pGEX6p1	(Mansour et al., 2014)

Strains used in this study

bacterial strain
BL21 (DE3)
BL21 (DE3) T7 Express
E. coli B F- *dcm ompT hsd*S(rB-mB-), *gal* λ(DE3)
yeast strain
YTX105 *Δcue1::HIS3, trp1-1 (am), his3-Δ200, ura3-52, lys2-801, leu2-3, -112,* matα (Biederer et al., 1997)

YTX106 *Δubc7::LEU2, trp1-1 (am), his3-Δ200, ura3-52, lys2-801, leu2-3, -112,* matα (Lenk & Sommer, 2000)

SUPPLEMENTAL EXPERIMENTAL PROCEDURES

Protocol used for ubiquitin chain synthesis and purification:

Reactions producing K48-linked chains included 1 μM E1 (Ube1), 20 μM Cdc34, 900 μM Ub and 600 μM Ub 6xHis$^{C-terminal}$ in 20 mM ATP, 0.9 mM DTT, 9 mM MgCl$_2$ and 50 mM Tris/HCl pH 8. Reactions for K63-linked chain assembly included 1 μM E1 (Ube1), 8 μM Ubc13, 8 μM Uev1a, 1200 μM Ub and 800 μM Ub 6xHis$^{C-terminal}$ in 20 mM ATP, 0.9 mM DTT, 9 mM MgCl$_2$ and 50 mM Tris/HCl pH 8.

Assembly of diubiquitin with distal or proximal ^{15}N-labeled moiety required modified *in vitro* reactions. K48-linked diubiquitin was assembled by 2 μM E1 (Ube1), 40 μM Cdc34, 750 μM Ub K48R and 750 μM Ub 6xHis$^{C-terminal}$ (one or the other ubiquitin variant ^{15}N-labeled) in 20 mM ATP, 0.9 mM DTT, 9 mM MgCl$_2$ and 50 mM Tris/HCl pH 8. K63-linked diubiquitin formation reactions consisted of 2 μM E1 (Ube1), 10 μM Ubc13, 10 μM Uev1a, 1000 μM Ub K63R and 1000 μM Ub 6xHis$^{C-terminal}$ (one or the other ubiquitin variant ^{15}N-labeled) in 20 mM ATP, 0.9 mM DTT, 9 mM MgCl$_2$ and 50 mM Tris/HCl pH 8.

Ubiquitin chain formation reactions were incubated at 37 °C for 18 h. Hexahistidine tagged chains were isolated using IMAC (Talon, Clontech Laboratories, Inc). Ubiquitin species of the IMAC eluate were separated by gel filtration in PBS, pH 7.5 and concentrated. Tetraubiquitin containing single ubiquitin variants were assembled by iterative chain assembly and purification. Chain elongation reactions included 100 μM preassembled chains and 75 μM monoubiquitin wild type or variant.

NMR structure determination:

NMR spectra were acquired on Bruker Avance spectrometers operating at proton frequencies ranging from 500 to 800 MHz. Resonances of uniformly ^{13}C-^{15}N-labeled Cue1$^{45-115}$ for structure calculation were assigned using a standard set of 3D triple resonance spectra. NOE distance restraints were obtained by automatic NOESY cross peak assignment and calibration using the program CYANA (Herrmann et al., 2002; Güntert, 2009) based on 3D ^{15}N-resolved NOESY-HSQC and ^{13}C-resolved NOESY-HSQC spectra. Backbone dihedral angle restraints were obtained using the TALOS+ software (Shen et al., 2009) and hydrogen bond constraints were derived from a 3D long-range BEST-[^{15}N,^{1}H]-TROSY-HNCO spectrum. The structure calculation was performed with CYANA using 100 random starting conformers, and 10,000 torsion angle dynamic steps per conformer. The 20 structures with the lowest target function values were selected for refinement. Restrained energy refinement was carried out using the OPALp program (Koradi et al., 2000).

SUPPLEMENTAL REFERENCES

Bagola, K., Delbrück, M. von, Dittmar, G., Scheffner, M., Ziv, I., Glickman, M.H., Ciechanover, A., and Sommer, T. (2013). Ubiquitin binding by a CUE domain regulates ubiquitin chain formation by ERAD E3 ligases. Mol. Cell *50*, 528–539.

Berndsen, C.E., and Wolberger, C. (2011). A spectrophotometric assay for conjugation of ubiquitin and ubiquitin-like proteins. Analytical Biochemistry *418*, 102–110.

Biederer, T., Volkwein, C., and Sommer, T. (1997). Role of Cue1p in ubiquitination and degradation at the ER surface. Science *278*, 1806–1809.

Güntert, P. (2009). Automated structure determination from NMR spectra. European Biophysics Journal EBJ *38*, 129–143.

Herrmann, T., Güntert, P., and Wüthrich, K. (2002). Protein NMR structure determination with automated NOE assignment using the new software CANDID and the torsion angle dynamics algorithm DYANA. Journal of Molecular Biology *319*, 209–227.

Koradi, R., Billeter, M., and Güntert, P. (2000). Point-centered domain decomposition for parallel molecular dynamics simulation. Computer Physics Communications *124*, 139–147.

Lenk, U., and Sommer, T. (2000). Ubiquitin-mediated proteolysis of a short-lived regulatory protein depends on its cellular localization. J. Biol. Chem. *275*, 39403–39410.

Mansour, W., Nakasone, M.A., Delbrueck, M. von, Yu, Z., Krutauz, D., Reis, N., Kleifeld, O., Sommer, T., Fushman, D., and Glickman, M.H. (2014). Disassembly of Lys11- and mixed-linkage polyubiquitin conjugates provide insights into function of proteasomal deubiquitinases Rpn11 and Ubp6. J. Biol. Chem. *290*, 4688-4704.

Rogov, V.V., Rozenknop, A., Rogova, N.Y., Löhr, F., Tikole, S., Jaravine, V., Güntert, P., Dikic, I., and Dötsch, V. (2012). A universal expression tag for structural and functional studies of proteins. Chembiochem *13*, 959–963.

Shen, Y., Delaglio, F., Cornilescu, G., and Bax, A. (2009). TALOS+: a hybrid method for predicting protein backbone torsion angles from NMR chemical shifts. Journal of Biomolecular NMR *44*, 213–223.